

Similarity normalization method for thermal conductivity depth profile reconstructions from inhomogeneous cylindrical and flat solids using thermal waves

Liwang Liu,¹ Chinhua Wang,^{1,a)} Xiao Yuan,¹ and Andreas Mandelis²

¹*Institute of Modern Optical Technologies, Soochow University, Suzhou, Jiangsu 215006, People's Republic of China*

²*Department of Mechanical and Industrial Engineering, Center for Advanced Diffusion-Wave Technologies, University of Toronto, Toronto, Ontario M5S 3G8, Canada*

(Received 13 November 2009; accepted 6 December 2009; published online 2 March 2010)

A similarity normalization method for thermal-wave depth profiling of layered and radial continuously varying inhomogeneous thermophysical properties in cylindrical solids is investigated and related to that developed for inhomogeneous flat solids both theoretically and experimentally using photothermal radiometry. The deconvolution of the curvature effect out of the overall thermal-wave field of inhomogeneous cylindrical solids allows conventional rectilinear thermal-wave inverse-problem techniques to be applied to thermal conductivity depth profile reconstructions in layered and inhomogeneous depth-varying cylindrical solids and opens new possibilities for depth profilometry of such solids using existing flat-surface inverse techniques.

© 2010 American Institute of Physics. [doi:10.1063/1.3285413]

I. INTRODUCTION

For decades, research on laser-induced photothermal radiometry (PTR) has been restricted to samples with flat surfaces due to the simplicity of geometry and of the relevant mathematical algorithms.¹⁻⁴ Significant progress has been made recently on curvilinear surfaces (samples) stimulated by increasing industrial applications, in which cylindrical and spherical samples were investigated.⁵⁻¹¹ Wang *et al.*⁵⁻⁸ developed mathematical models of homogeneous and two-layer cylindrical and spherical samples using Green's function methods, in which the dependence of the PTR signal on geometrical and thermophysical parameters of the curvilinear samples was studied. Salazar *et al.*⁹⁻¹¹ further developed the theory of multilayer cylindrical and spherical solids for the characterization of surface structures with discrete or continuously varying thermophysical properties using the quadrupole method¹² and also showed the explicit dependence of thermal-wave fields on both geometrical and thermophysical properties. These investigations laid the groundwork on which the thermophysical properties of curvilinear (cylindrical and spherical) solid samples can be characterized. In terms of practical applications of the curvilinear theoretical models, however, several aspects must be considered. The complicated mathematical dependence on the geometrical and thermophysical properties (such as thermal conductivity /diffusivity, and/or case-depth hardness, etc.) require foreknowledge of the precise values of all the geometrical dimensions which may have significant impact on measurement accuracy of thermophysical properties. Difficulties with further developing an inverse problem for retrieving the thermophysical depth profile may be encountered due to the complexity of the algorithm for the

curvilinear surfaces. In addition, various arbitrary geometries of practical samples (cylindrical and spherical surfaces are just the simplest cases of curvilinear samples) require a curvature-independent technique before inverse photothermal methodologies such as PTR can be put to use in real industrial settings. In this paper, we introduce and demonstrate theoretically and experimentally a thermal-wave similarity normalization method applicable to solid cylinders with layered and continuously variable thermophysical depth profiles as well as flat solids with arbitrary inhomogeneous depth profiles. The similarity-normalized PTR signals from cylindrical solids are shown to be equivalent to those of a similarity-normalized flat solid of the same material with the same inhomogeneous thermophysical depth profile, thereby opening new possibilities for quantitative inverse-problem reconstruction of arbitrary thermal-conductivity depth profiles in curvilinear solids and defining the conditions of the validity of the similarity normalization method.

II. THEORETICAL

The physical mechanism for the elimination or deconvolution of the geometrical (curvature) effect out of the total thermal-wave signal, in its simplest form, can be understood from the mathematical similarity of the thermal-wave theory in single-layer (uniform) and multilayered (simplest case: two-layered) cylindrical solids.⁵⁻⁸ The same applies to spherical solids which, however, will not be discussed further here. As an illustration of the mathematical and physical mechanism at work in the simplest cylindrical case, the thermal-wave expression for a single-layer cylinder and a two-layer cylinder is given in the form of Eqs. (1) and (2), respectively,^{5,6}

^{a)}Author to whom correspondence should be addressed. Electronic mail: chinhua.wang@suda.edu.cn.

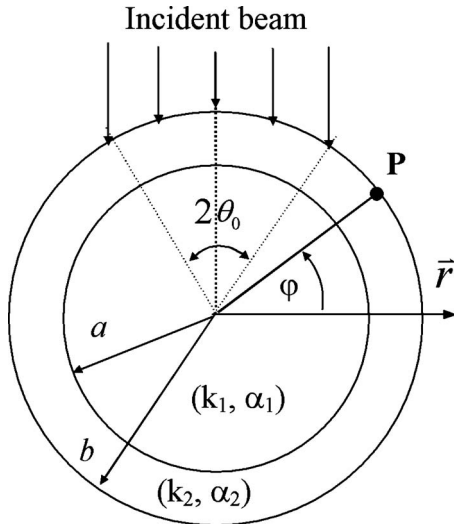


FIG. 1. Geometry showing the cylindrical coordinate system with angular coordinates (φ, θ_0) .

$$T(r, \varphi, \omega) = A_1 \left\{ \frac{2I_0(\sigma r)}{I'_0(\sigma b)} F_1(\theta_0) + \frac{I_1(\sigma r)}{I'_0(\sigma b)} F_2(\theta_0, \varphi) + 2 \sum_{m=2}^{\infty} \frac{I_m(\sigma r)}{I'_m(\sigma b)} F_3(\theta_0, \varphi) \right\}, \quad (1)$$

$$T(r, \varphi, \omega) = A_2 \left\{ \frac{2\Xi_0(r, \omega)}{I'_0(\sigma_2 b)} F_1(\theta_0) + \frac{\Xi_1(r, \omega)}{I'_0(\sigma_2 b)} F_2(\theta_0, \varphi) + 2 \sum_{m=2}^{\infty} \frac{\Xi_m(r, \omega)}{I'_m(\sigma_2 b)} F_3(\theta_0, \varphi) \right\}, \quad (2)$$

where A_1 and A_2 are parameter-independent constants, $\sigma(\omega) = (i\omega/\alpha)^{1/2}$ is the thermal wave number, $I_m(z)$ ($m = 0, 1, \dots$) is the complex-argument modified Bessel function of the first kind of order m , and $I'_m(z)$ is its derivative; $\Xi_m(r, \omega)$ are constants related to the thermal conductivities of the outer and inner cylindrical layers; b is the radius of the single-layer cylinder as well as the outer radius of the two-layer cylinder. These functional groups carry the effects of depth inhomogeneity in the thermal-wave fields of composite solids. $F_1(\theta_0)$, $F_2(\theta_0, \varphi)$, and $F_3(\theta_0, \varphi)$ in both Eqs. (1) and (2) are only functions of the cylindrical angular coordinates: the azimuthal angle φ of the measurement point P, Fig. 1, and θ_0 , the half angle subtended by the illumination beam. From Eqs. (1) and (2) it is seen that the mathematical expressions of the thermal-wave field from uniform and two-layer cylindrical samples are *similar*, the only difference being the $\Xi_m(r, \omega)$ -related terms which act as coefficients of the aforementioned same angular functions. The similarity normalization method is based on the fact that the normalization of the two-layer (and, by extension, arbitrarily inhomogeneous layer) cylinder expression, Eq. (2), by that of the homogeneous single-layer cylinder of the same material and radius, Eq. (1), very effectively compensates for the effects of curvature as manifested by functions F_1 , F_2 , and F_3 , on the resulting expressions when normalized with the frequency dependence of the same flat solid with a homogeneous depth

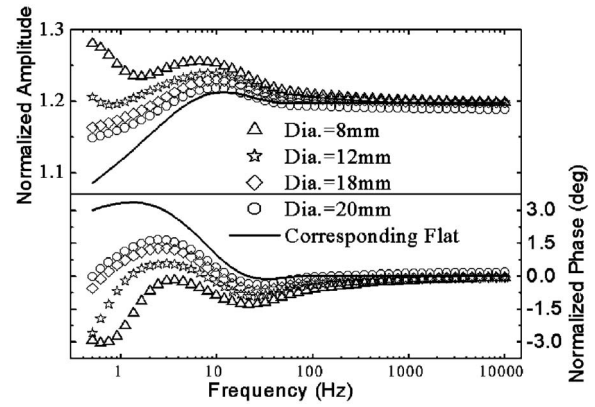


FIG. 2. Conventional normalized thermal-wave amplitude and phase of two-layer cylinders with various diameters. a : inner radius, b : outer radius, k_i : thermal conductivity, and α_i : thermal diffusivity.

profile. For comparison, Fig. 2 shows the conventional signal amplitude and phase of two-layer cylinders with various diameters normalized with that of a semifinite flat sample of the same materials as the core layer of the cylinder counterparts. The corresponding two-layer flat solid similarity normalization to the semifinite flat solid homogeneous (single-layer) counterpart is also shown in Fig. 2. In the calculation, thermal conductivity and diffusivity of the thin layer (2) and the inner core part (1, also representing those of the single-layer) were $k_2 = 36.05$ W/mK, $\alpha_2 = 9.426 \times 10^{-6}$ m²/s, $k_1 = 51.9$ W/mK, and $\alpha_1 = 13.57 \times 10^{-6}$ m²/s, respectively. The measurement angle was $\varphi = 45^\circ$. A set of cylinders with (outer) radius of curvature ranging from 4 to 10 mm was examined. All cylinders had fixed thickness of the exterior (top) layer $L_0 = 0.6$ mm. Figure 2 shows that both amplitude and phase are very sensitive to the radius of curvature of the cylinders and they deviate significantly from that of the corresponding flat surface of the same layered structure (solid line). Figure 3 shows the curvature elimination effect based on the one- and two-layer cylindrical models using the similarity normalization method. To quantitatively show the elimination effect, average deviation factors are defined, $\Delta_X = \sqrt{\sum_{j=1}^N (X_{j,\text{cylinder}} - X_{j,\text{flat}})^2} / N / (X_{\text{max}} - X_{\text{min}})_{\text{flat}}$, which represent the average deviation (in percent) from the corresponding similarity-normalized flat surface in either ampli-

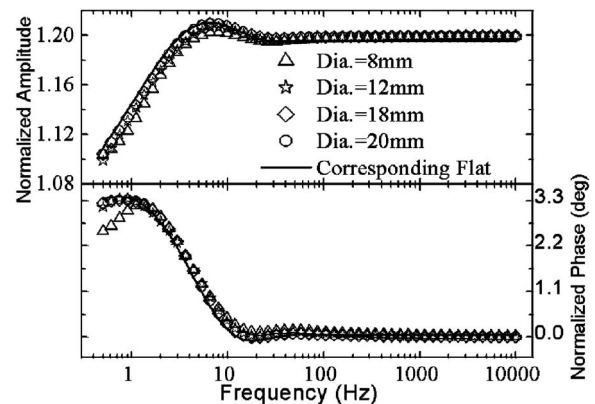


FIG. 3. Similarity normalization method applied to two-layer cylinders and flat samples with fixed thickness of the outer layer ($L_0 = 0.6$ mm) and various diameters.

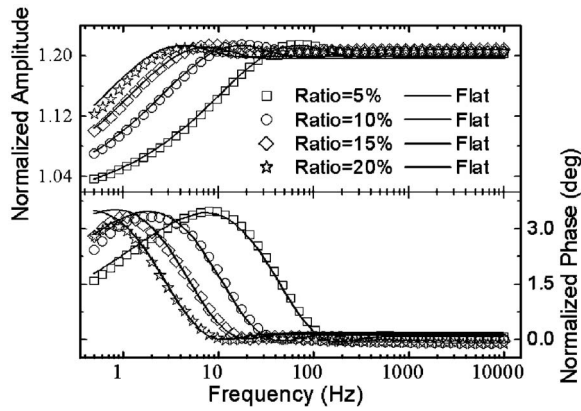


FIG. 4. Theory of similarity normalization for a set of two-layered cylinders with fixed radius ($b_{2L}=5$ mm) and various thicknesses of the outer thin layer. Symbols: cylindrical surface and solid lines: flat surface.

tude and phase channel ($X=A$, ϕ , respectively). $N=51$ is the number of frequency scanned points. In Fig. 3, Δ_A is 4.8%, 3.8%, 2.6%, and 2.4%, whereas Δ_ϕ is 5.0%, 2.6%, 2.0%, and 1.8% for Dia.=8 mm, 12 mm, 18 mm, and 20 mm, respectively. It is obvious that all deviations are small ($<5\%$) and all normalized curves overlap with the flat surface, which is also borne out by experimental observations, Fig. 7(a). Physically, the similarity normalization method acts to minimize or eliminate the effects of distortion by the surface curvature of the equiphase thermal waveforms generated within a diffusion length from the optically irradiated curvilinear surface through amplitude and phase compensation by a homogeneous solid of the same curvature. In its broadest sense the method includes inhomogeneous flat solids (zero curvature) normalized by the thermal-wave frequency responses of their bulk-homogeneous counterparts.

Although accurate to $\geq 95\%$ over a wide range of curvatures, Fig. 3, the validity range of similarity normalization in suppressing the effects of geometrical factors from the overall thermal-wave frequency responses depends mainly on the relative values of the cylindrical diameter and the thickness of the top (inhomogeneous) layer. This is demonstrated in Fig. 4 which shows the similarity normalization for a set of cylinders with fixed outer radius ($b=5$ mm) and various thicknesses of the outer thin layer, including the frequency response of the corresponding flat surface with the same (two-layer) material depth profile structure. An inhomogeneity ratio $\chi \equiv (b-a)/b$ can be defined, where b is the outer radius and a is the inner radius of the cylinder. In the calculation, the thermophysical parameters of the two-layer cylinder were the same as those used in Fig. 3. For $\chi=5\%$, 10%, 15%, and 20% the amplitude deviation Δ_A between the cylinders and the corresponding flat solid is 1.5%, 3.1%, 5.3%, and 8.9%, respectively, and the phase deviation Δ_ϕ is 2.2%, 3.1%, 3.7%, and 5.0%, respectively. It is seen that different outer-layer thicknesses ($b-a$) give proportionately different deviations: The larger the ratio χ , the greater the deviation, which, according to Fig. 4, mainly appears at very low frequencies $f < 3$ Hz. Below that frequency the thermal diffusion length becomes comparable to the radius of curvature and the thermal waveform becomes maximally distorted by the curvature. The validity range of the technique in which a

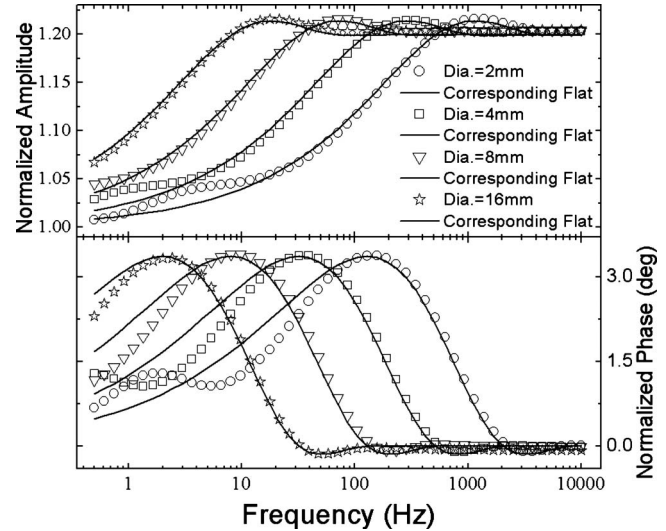


FIG. 5. Similarity normalization for a set of two-layered cylinders with the same ratio χ but different radii and thicknesses of the outer thin layer. Symbols: cylindrical surface and solid lines: flat surface.

maximum ratio χ is allowed depends on the experimental uncertainty and/or the acceptable tolerance (whichever is larger) of the deviation between the similarity-normalized cylindrical solid and the corresponding flat solid of the same material. Typically, if the experimental uncertainty or the acceptable tolerance is 5%–10%, the ratio χ limit for deviation containment within 5%–10% is approximately 15%–20%, i.e., for a 5 mm radius cylinder the outer-layer thickness limit is ~ 1 mm, which is a typical case of hardness depth in the heat treating industry.

The validity frequency range of the similarity normalization procedure depends on the thickness of the inhomogeneous top layer of the sample. Figure 5 shows the effect of different top-layer thicknesses and different radii of curvature at fixed ratio factor χ on the behavior of the photothermal signals. In Fig. 5, the ratio χ is fixed at 12%, the external radius of curvature b is 1, 2, 4, and 8 mm, and the corresponding top-layer thickness is 0.12, 0.24, 0.48, and 0.96 mm, respectively. The corresponding photothermal signal of the flat solid with the same top-layer thickness as those of the cylinders is also shown in the figure (solid line). The peak/valley positions in both amplitude and phase shift with the top-layer thickness despite the fixed χ ratio. As expected, the thicker the top layer, the lower the frequency of the peak. This phenomenon can be explained by the larger thermal diffusion length (lower frequency) required to detect the thicker coating layer through interlayer thermal-wave interference. The similarity-normalized amplitude and phase of the cylinders (symbols in the figure) follow the same pattern as the flat surface. The curves of the normalized cylinders and the corresponding flat well overlap over certain frequencies as seen in Fig. 5. The overall deviation between the cylinders and the corresponding flat solids over the entire frequency range increases as the diameter of the cylinder decreases. However, significant deviations occur only in frequency ranges below the phase peaks. For frequencies higher than those of the phase peaks deviations are minimal and nonmeasurable in practice, in the presence of experimental

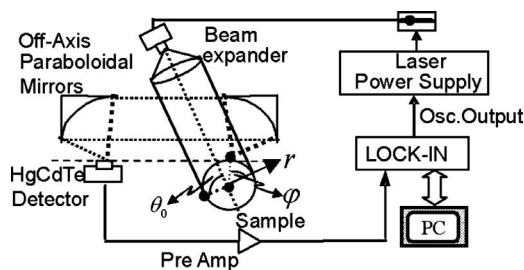


FIG. 6. Experimental PTR setup.

error. This conclusion is valid for all curves with the same ratio χ , provided that χ is limited within a certain range, e.g., 20%, in the context of Fig. 4 which encompasses all important material inhomogeneity depth profiles in cases like industrial steel case hardness. These observations suggest that the peak phase frequency (which is determined by the thickness of the top layer) can be used as a rigorous validity limit criterion of the similarity normalization frequency range to achieve optimal results when the method is employed.

III. EXPERIMENTAL AND RESULTS

The experimental PTR setup has been described elsewhere^{5,6} and is also shown in Fig. 6. Briefly, the optical excitation source was a high-power semiconductor laser, the frequency of which was modulated by a periodic current driver. The harmonic infrared radiation from the sample surface was collected by an off-axis paraboloidal mirror system and detected by an HgCdTe detector (EG&G Judson). The signal from the detector was preamplified and then fed into a lock-in amplifier (EG&G Instruments) interfaced with a personal computer. Two sets of cylindrical AISI1020¹³ steel samples (composition: 0.18%–0.23% C, 0.3%–0.6% Mn) were machined with radii ranging from 2 to 10 mm. One set of samples underwent a case hardening (carburizing) process as one batch to assure the same case depth profile, with a nominal case depth of 0.04 in. The actual case depth was measured using the conventional mechanical indentation method. The other set was kept unhardened as a uniform reference. Samples of the same size were positioned carefully at the focal point of the paraboloidal mirror. Top and bottom flat surfaces of the 16 mm-diameter cylindrical sample were also measured in the same geometry. The signals from the unhardened and hardened sample surfaces of the same diameter were then normalized. Figure 7(a) shows the normalized experimental results for samples with diameters 4, 10, and 16 mm, and those from the flat solid of diameter 16 mm. The hardened samples substantially behave as two-layer cylinders with an effective upper layer thickness approximately equal to the case depth.¹⁴ It is seen that all normalized amplitudes and phases of the cylindrical solids with various diameters (curvatures) overlap with those of the corresponding flat solid similarity-normalized with a homogeneous version of the same flat solid. These results are in significant contrast to the sensitive behavior of the PTR signal to the radius of curvature of the samples^{5,7} and are in agreement with our theoretical and computational simulations. They suggest that an inhomogeneous cylindrical solid

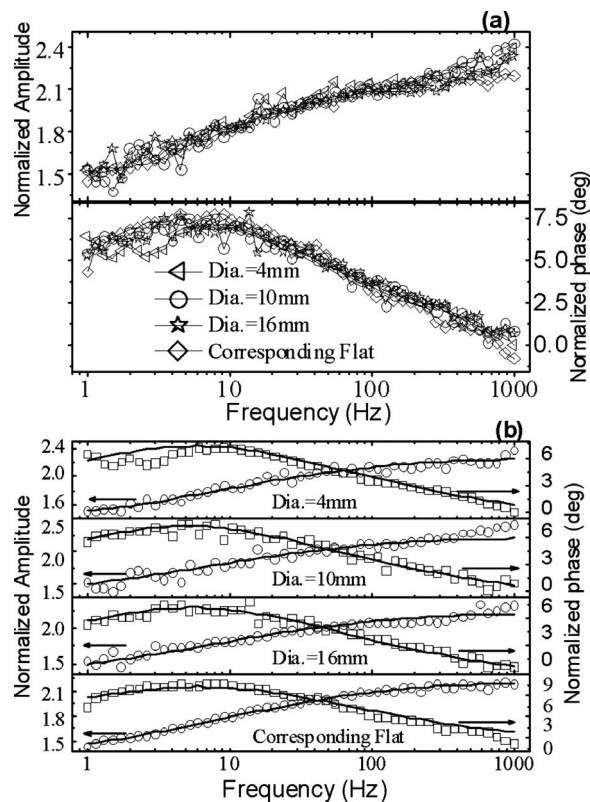


FIG. 7. (a) Experimental similarity-normalized amplitudes and phases of various hardened cylindrical steel rods (diameters $D=4, 10,$ and 16 mm) and the corresponding normalized flat solid frequency response with the same thermophysical property depth profile. (b) Comparison of theoretical best-fits (lines) and experimental data (symbols). The best-fit results are as follows: 4 mm cylinder: $k_1=15.55$ W/mK, $L_0=0.95$ mm, and $q=4805$ mm⁻¹; 10 mm cylinder: $k_1=15.93$ W/mK, $L_0=0.98$ mm, and $q=3475$ mm⁻¹; 16 mm cylinder: $k_1=15.79$ W/mK, $L_0=1.02$ mm, and $q=3666$ mm⁻¹; flat solid: $k_1=15.43$ W/mK, $L_0=1.08$ mm, and $q=3975$ mm⁻¹.

can be characterized using algorithms developed for inhomogeneous rectilinear solids.¹⁵ This is an important result since the complicated dependencies of the thermal-wave signal on both geometrical and thermophysical parameters have prevented the use of thermal-wave techniques for quantitative inverse-problem depth profile reconstructions of curvilinear solids to date.

IV. THERMOPHYSICAL DEPTH PROFILE RECONSTRUCTIONS

Thermal conductivity depth profile reconstructions of various cylindrical samples were performed using our flat-surface algorithm.¹⁵ Figure 7(b) shows the best-fit results. In the fitting, the depth coordinate (z)-dependent thermal conductivity of the case hardened steel cylinders was assumed to vary continuously with the form^{3,14,15} $k(z)=k_1[(1+\Delta e^{-qz})/(1+\Delta)]^2$ and $\Delta=(1-\sqrt{k_N/k_1})/(\sqrt{k_N/k_1}-e^{-qL_0})$, where k_1 and k_N represent the values of the thermal conductivity at the two boundary surfaces $z=0$ (surface of the cylinder) and L_0 , respectively. L_0 is the effective outer-layer depth at which the thermal conductivity reaches the saturation value k_N , i.e., the conductivity of the unhardened center of the cylinder. From Fig. 7(b) it is seen that both amplitudes and phases of all samples are very well fitted for di-

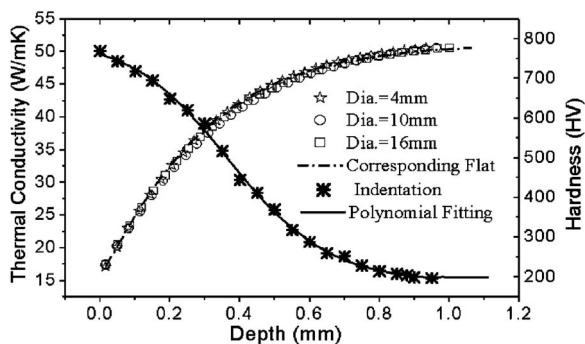


FIG. 8. Reconstructed depth profiles of thermal conductivity of hardened cylindrical steel rods and the corresponding flat solid reconstruction under the same carburizing treatment.

ameters between 4 and 16 mm. The theory used for fitting the data is given by Eq. (6) of Ref. 15. When the diameter is small ($D=4$ mm), it is seen that the deviation between the theory and the experiment in the low-frequency range (<10 Hz) is maximum due to the residual curvature effect, as expected. The reconstructed thermal conductivity curves, $k(z)$, of the cylindrical solids are shown in Fig. 8. The application of the similarity normalization has resulted in near-coincidence of all $k(z)$ depth profiles independently of the cylindrical curvature and reflects the success of the method in reconstructing arbitrary steel-hardness depth profiles. Figure 8 also shows the microhardness profiles (right axis), obtained with the conventional destructive mechanical indentation method. The thermal conductivity profile reconstruction exhibits good anticorrelation with the indenter-generated profiles, as expected.²⁻⁴ The saturation thickness L_0 of all four samples is about 1.0 mm which is also consistent with the independently and destructively measured microhardness depth profiles.

V. CONCLUSIONS

In summary, we have demonstrated a similarity normalization method of thermal-wave fields in inhomogeneous cylindrical solids which yields frequency-scan similarity to that from a flat solid of the same material and inhomogeneous thermophysical depth profile as the cylinders. The similarity normalization method is significant for the depth profilometric characterization of the thermophysical properties of curvilinear solids using thermal waves, which, at present, is limited to flat solids only. Although the similarity normalization method is demonstrated only for cylinders in this paper, the

physical underpinnings of the normalization technique, based on distortion compensation of thermal waveforms confined within the curvilinear matrix, lead to the conclusion that the method may find applications with broader families of curvilinear solids of arbitrary shapes. The theoretical validity criterion for the technique is that the ratio of the inhomogeneous layer depth to the limiting radius of curvature (i.e., the smallest radius of curvature in all directions) of the curvilinear geometry should be <1 , typically 15%–20%, which corresponds to an accuracy $\geq 90\%$ of the similarity normalization method. The experimental validity criterion for applying the technique to frequency scans is that the low-frequency limit must be set at the interferometric peak of the thermal-wave phase. The resulting degree of accuracy was found to be excellent for reconstructing thermophysical depth profiles from curvilinear solids using rectilinear inverse-problem methodologies.

ACKNOWLEDGMENTS

This work has been sponsored by the National Natural Science Foundation of China (No. 60877063) and the Scientific Research Foundation for the Returned Overseas Chinese Scholars, State Education Ministry of China. X.Y. acknowledges the support of NSAF (Nos. 10676010 and 10876011). One of us (A.M.) is grateful to the Canada Research Chairs program for support.

- ¹D. P. Almond and P. M. Patel, *Photothermal Science and Techniques* (Chapman and Hall, London, 1996).
- ²T. T. N. Lan, H. G. Walther, G. Goch, and B. Schmitz, *J. Appl. Phys.* **78**, 4108 (1995).
- ³M. Munidasa, F. Funak, and A. Mandelis, *J. Appl. Phys.* **83**, 3495 (1998).
- ⁴H. G. Walther, D. Fournier, J. C. Krapez, M. Luukkala, B. Schmitz, C. Sibilila, H. Stamm, and J. Thoen, *Anal. Sci.* **17**, 165 (2001).
- ⁵C. Wang, A. Mandelis, and Y. Liu, *J. Appl. Phys.* **96**, 3756 (2004).
- ⁶C. Wang, A. Mandelis, and Y. Liu, *J. Appl. Phys.* **97**, 014911 (2005).
- ⁷C. Wang, Y. Liu, A. Mandelis, and J. Shen, *J. Appl. Phys.* **101**, 083503 (2007).
- ⁸G. Xie, Z. Chen, C. Wang, and A. Mandelis, *Rev. Sci. Instrum.* **80**, 034903 (2009).
- ⁹A. Salazar, F. Garrido, and R. Celorrio, *J. Appl. Phys.* **99**, 066116 (2006).
- ¹⁰A. Salazar and R. Celorrio, *J. Appl. Phys.* **100**, 113535 (2006).
- ¹¹R. Celorrio, A. Mendioroz, E. Apiñaniz, A. Salazar, C. Wang, and A. Mandelis, *J. Appl. Phys.* **105**, 083517 (2009).
- ¹²D. Maillat, S. André, J. C. Batsale, A. Degiovanni, and C. Moyne, *Thermal Quadrupoles* (Wiley, New York, 2000).
- ¹³R. Steiner, *Metals Handbook*, 10th ed. (ASM International, Materials Park, OH, 1990), Vol. 1, p. 196.
- ¹⁴A. Mandelis, F. Funak, and M. Munidasa, *J. Appl. Phys.* **80**, 5570 (1996).
- ¹⁵H. Qu, C. Wang, X. Guo, and A. Mandelis, *J. Appl. Phys.* **104**, 113518 (2008).